DOI: 10.1002/ ((please add manuscript number))
Article type: Full Paper

Second order optical nonlinearity in silicon waveguides - inhomogeneous stress and interfaces

Clemens Schriever, Federica Bianco, Massimo Cazzanelli, Mher Ghulinyan, Christian Eisenschmidt, Georg Schmidt, Johannes de Boor, Alexander Schmid, Johannes Heitmann, Lorenzo Pavesi, Jörg Schilling**

Dr. C. Schriever
Centre for Innovation Competence SiLi-nano, Martin-Luther-University Halle-Wittenberg, Karl-Freiherr-von-Fritsch-Str. 3, 06120 Halle (Saale), Germany
E-mail: clemens.schriever@physik.uni-halle.de

Dr. F. Bianco, Dr. M. Cazzanelli
Nanoscience Laboratory, Department of Physics, University of Trento, via Sommarive 14, 38123 Povo, Trento, Italy

M. Ghulinyan
Advanced Photonics and Photovoltaics, Centre of Materials and Microsystems, Bruno Kessler Foundation, via Sommarive 18, 38123 Povo, Trento, Italy

Dr. C. Eisenschmidt, Prof. G. Schmidt
Institute of Physics, Martin-Luther-University of Halle-Wittenberg, Heinrich-Damerow-Str. 4, 06120 Halle (Saale), Germany

Dr. J. de Boor
Max Planck Institute of Microstructure Physics, Weinberg 2, 06120 Halle (Saale), Germany

A. Schmid, Prof. J. Heitmann,
Institut für Angewandte Physik, TU Bergakademie Freiberg, Leipziger Str. 23, 09599 Freiberg, Germany

Prof. L. Pavesi
present address: NEST, Istituto Nanoscienze-CNR and Scuola Normale Superiore, P.za S. Silvestro 12, 56127 Pisa, Italy

Jun.Prof. J. Schilling
Centre for Innovation Competence SiLi-nano, Martin-Luther-University Halle-Wittenberg, Karl-Freiherr-von-Fritsch-Str. 3, 06120 Halle (Saale), Germany
E-mail: joerg.schilling@physik.uni-halle.de

Keywords: second harmonic generation, inhomogeneous strain, symmetry breaking, silicon

Abstract: The lack of a dipolar second order susceptibility ($\chi^{(2)}$) in silicon due to the centrosymmetry of its diamond lattice usually inhibits efficient second order nonlinear optical

processes in the silicon bulk. Recently the deposition of stressed silicon nitride layers and the corresponding inhomogeneous strain in silicon led to the demonstration of second harmonic generation and electro-optic modulation in strained silicon waveguides. However, the respective impact of the stress/strain gradient and the involved interfaces were not clear. Here, we investigate the influence of the stress and the stressing silicon nitride layer using second harmonic generation measurements in transmission. The results show, that the enhancement of the second order nonlinearity arises from a constructive superposition of stress-induced and interface-related effects. Particularly, the stress gradient in silicon breaks the symmetry of the crystal lattice, while positive fixed charges at the silicon/silicon nitride interface are responsible for a pronounced electric-field-induced-second harmonic (EFISH) contribution. These results demonstrate the impact of external factors for the creation of an effective $\chi^{(2)}$ in materials and open new perspectives for the use of second order nonlinear optical processes in silicon photonics.

1. Introduction

Although silicon photonics became an established technology in the last years, nonlinear optical processes like difference frequency generation or ultrafast electro-optic modulation using the linear electro-optic effect are not possible in silicon. On a fundamental level this is caused by the centrosymmetry of the silicon crystal lattice, which results in a lack of a dipolar bulk $\chi^{(2)}$. Therefore, nonlinear active devices based on silicon are usually fabricated by exploiting its third order nonlinearity $\chi^{(3)}$ [1] or combining various nonlinear materials with silicon [2-4]. However, since silicon exhibits a strong two-photon absorption in the near infrared, the efficiency of these processes is limited. Of specific interest were also situations where the centrosymmetry of bulk the silicon crystal is broken and a nonzero $\chi^{(2)}$ is induced e.g. at free surface or an interface [5-8]. This lead to efforts to deform the silicon lattice

deliberately using inhomogeneous strain e.g. through a deposition of a stressing layer [9-11]. Recently, the stressing layer method was used to demonstrate second harmonic generation (SHG) [12]and electro-optical modulation [13], [14] in strained silicon waveguides. In both cases a silicon nitride (SiN_x) overlayer was used to induce the stress inside the silicon waveguide core. On the other hand, second order nonlinearities were also observed from silicon nitride itself [15-19]. In view of this, the different impact of interface, stress and nature of the overlayer on the second order nonlinearity is not clarified yet.

Here, we investigate the influence of the stress and the existence of a silicon nitride overlayer on the second order nonlinear response of strained silicon waveguides. We will show a direct correlation of the integrated stress gradient in the silicon lattice (which is a measure of the breaking of the centrosymmetry of the Si-lattice) with the conversion efficiency for second harmonic generation. In addition we discuss the impact of the silicon nitride cover layers and, specifically, of their interface with Si. For this purpose a set of silicon-on-insulator waveguide samples was investigated under various conditions of mechanical stress.

2. Inhomogeneously strained Si-Waveguides

An overview of the different sample structures is given in **Figure 1** and **Table 1.** All waveguides were fabricated from SOI wavers with a 2µm thick p-type device layer (ρ=2.4 Ohm*cm, N_A= 7x10^{15} cm^{-3}). The set consists of a reference sample *SiRef* with uncoated 2µm thick Si-strip waveguides resting on a buried oxide layer of the same thickness. Furthermore, a sample *SiO2* (Fig. 1a), whose waveguides were covered with a layer of stressing thermal oxide, was produced. A comparison of the second harmonic (SH) conversion efficiencies of both samples can be used to study the impact of the stress on the second order nonlinearity without any effect from a SiN_x-layer. Additionally, samples with silicon nitride overlayers of different stress conditions were produced. Sample SiN0 was completely covered with a thin

almost unstressed SiN_x-overlayer to investigate the influence of the SiN_x layer alone, excluding any stress related effects. To examine the combination of SiN_x and the stress effect, additional silicon nitride coated samples were processed with different stress extent, stress sign and layer thicknesses.

To relate the second order response measured in the nonlinear transmission experiments with the stress state of the waveguides, a finite element method (FEM) model was employed to estimate the stress tensor across the waveguide cross section, where a plane stress regime was assumed [20],[21]. **Figure 2** shows the distribution of the normal stress component σ_{xx} and the local stress gradient (arrows) for 10μm wide waveguides of different samples. Moreover, based on the sp^3 orbital models in [10],[9], a linear relationship between the second order susceptibility $\chi^{(2)}$ and the stress gradient was assumed. A rigorous analysis would require the study of the influence of the local stress gradient on the local nonlinear optical properties of the waveguide core. However, the measurements of the second harmonic light in transmission represent a non-simple average of the local contributions along the waveguide cross section. Therefore, a total stress gradient was used to describe the overall stress inhomogeneity in the various samples. This was quantified by integrating the sum of the local gradients of the stress tensor components over the waveguide cross section as follows

$$\sum = \int \left(\left| \frac{\sigma_{xx}}{dx} \right| + \left| \frac{\sigma_{xx}}{dy} \right| + \left| \frac{\sigma_{yy}}{dx} \right| + \left| \frac{\sigma_{yy}}{dy} \right| + \left| \frac{\sigma_{xy}}{dx} \right| + \left| \frac{\sigma_{xy}}{dy} \right| \right) dA \qquad (1)$$

A comparison of the stress distribution in the samples *SiRef* and *SiN0* (Fig. 2a) and b)) shows, that the thin SiN_x cover layer has no influence on the stress inside the waveguide. On the contrary, the stress distribution is slightly affected by the stress in the underlying oxide layer that is created during the fabrication of the SOI wafer (Σ_{SiRef} = 436 N/m, Σ_{SiN0} = 383 N/m) [12],[22]. A stronger influence on the stress can be seen for the samples *SiN1* and *SiN2* with a stressed SiN_x layer on top (Fig. 2c) and d)). Both samples show almost the same Σ

(Σ_{SiN1}=1535 N/m, Σ_{SiN2}=1559 N/m). However, as both samples are coated with layers of different thickness and stress level, the local stress gradients differ strongly from each other. In Fig. 2e) the stress distribution in the SiO_2 coated sample is shown, exhibiting a strong total stress gradient of Σ_{SiO2} = 3197 N/m.

To test the reliability of the employed FEM model for the calculation of the stress gradients, the stress distribution in a reference system has been modeled. The system consists of (111) oriented, laser written [23] silicon grating structures, stressed by a 110 nm thermal SiO_2-layer (σ= -450 MPa). The numerical results were used to calculate artificial reciprocal space maps (RSM) for the Si-(111)-reflex, that were compared to experimental ones determined by high resolution x-ray diffraction (HRXRD). In comparison to the diffraction pattern of the unstrained grating (Fig. 3a)), the strained grating exhibits a bending of its diffraction pattern in Q_z-direction (Fig. 3c)).

The artificial RSMs were calculated using kinematic diffraction theory [24]. By this means the amplitude of the field scattered by a single ridge can be expressed as [25]

$$A_{ridge} = \sum_j F \exp\left[i\,\vec{Q}\cdot\left(\vec{r}_j + \vec{u}\left(\vec{r}_j\right)\right)\right] \qquad \textbf{(2)}$$

The ridge is split into identical unit cells (10 x 10 atoms) with a form-factor *F* located at the position $\vec{r}_j + \vec{u}\left(\vec{r}_j\right)$. Here $\vec{r}_j$ describes the position of the cell in the unstressed case while $\vec{u}\left(\vec{r}_j\right)$ represents the additional displacement of the respective cell due to the local strain. The data for the position of the displaced unit cells was taken from the FEM model that was calculated using the actual parameters of the sample.

For the artificial RSM the contribution of several ridges was taken into account by summing over the contribution of *N* single ridges separated by a lattice constant Γ:

$$A_{total} = A_{ridge}\cdot\left(1 + e^{i\,Q_x\Gamma} + \ldots + e^{i\,Q_x N\,\Gamma}\right) = A_{ridge}\cdot\frac{e^{i\,Q_x(N+1)\Gamma}-1}{e^{i\,Q_x N\,\Gamma}-1} \qquad (3)$$

A comparison between the experimentally determined and calculated RSM (Fig. 3a, c) and Fig.3b, d), respectively, shows a good agreement for both cases - the stressed and unstressed geometries. This result proves that the FEM model is suitable to represent the actual stress distribution inside a stressed silicon waveguide and that the calculated integrated stress gradient discussed above is reliable.

3. Second harmonic generation from Si waveguides

To investigate the second order nonlinear optical properties of the different samples, the SH signal from 2mm long waveguides was measured in transmission using a tunable laser source with 100 fs-pulses at a wavelength of about 2200 nm (Fig. 4). For one spectrum an average of over 1000 single measurements was taken. To reduce the error when estimating the intensity of the SH peak, a Gaussian curve was fitted to the spectrum (Fig. 4 Inset I). Inset II shows the typical linear dependence between the wavelengths of the second harmonic and fundamental beams proving that indeed the SHG process was observed.

As it was not possible to estimate the exact SH intensity, no absolute $\chi^{(2)}$ values could be calculated. Instead, a relative conversion efficiency η was determined, which allows a comparison of the second order nonlinearities of the different samples measured under identical conditions. It is defined as:

$$\eta = \frac{I_{2\omega}}{I_{\omega}^{2}} \tag{4}$$

that is the ratio between the SH intensity $I_{2\omega}$ and the squared excitation intensity I_ω. As the conversion efficiency was expected to be rather low, the effect of pump depletion was neglected here.

Figure 5 relates the estimated conversion efficiency η to the calculated total stress gradient Σ. To ensure confidence in the obtained values, η has been evaluated from at least three different

waveguides with identical parameters. The error bars result from the maximum semi-dispersion of the determined values. For sample *SiRef* only a weak SH signal was generated. It is caused by contributions from the waveguide surfaces and the interface between silicon and native and buried SiO_2 layers, where the centrosymmetry is locally broken. A clear increase of η was observed in the stressed SiO_2 covered sample (*SiO2*) (Fig. 5). In this sample the interface contributions can be considered comparable to the ones of sample *SiRef*, since also *SiRef* carries a natural oxide layer of a few nm thickness. Instead, analyzing the mechanical states of the two samples (Σ_{SiRef} = 436 N/m and Σ_{SiO2} = 3197 N/m), the sample *SiO2* shows a much larger total stress gradient, that indicates a stronger deformation of the Si-Si bonds in the crystalline lattice. The enhancement observed in the conversion efficiency can be thus attributed to the effect of the inhomogeneous stress inside the waveguide core, that agrees with earlier statements [12].

When studying the conversion efficiency of the samples coated with a stressing silicon nitride layer (Fig. 5), it can be seen that η increases when the stress gradient increases. This is particularly obvious for the strongly stressed *SiN2* sample. It has the same film thickness, but a very different stress level compared to the quasi unstressed *SiN0* sample. This confirms the existence of the stress related effect on $\chi^{(2)}$ also in the SiN_x-stressed samples.
To examine a possible nonlinear effect due to the SiN_x layer itself, the conversion efficiencies of *SiRef* and the silicon nitride covered (but quasi unstressed) sample *SiN0* were compared. For *SiN0* the conversion efficiency η is enhanced by a factor of approximately two compared to *SiRef*. This indicates an unexpectedly strong influence of the silicon nitride layer or its interface. In addition one notes, that this contribution adds constructively to the stress effect, leading to an overall stronger enhancement of the effective nonlinearity than in the case of sample *SiO2*. Additional support for the superposition of both effects (stress related and SiN_x-

related) is gained by adding the SiN_x layer contribution from sample *SiN0* to the conversion efficiency measured in sample *SiO2*. Interestingly, the resulting η value appears aligned with the trend observed for the other stressed SiN_x covered samples (diamond marker in Fig. 5). The origin of the strong SH signal in the quasi unstressed sample *SiN0* is indeed puzzling. From the presented results, we conclude that the reason for its increased SH-intensity has to lie within the SiN_x layer or the SiN_x/Si-interface. However results and interpretations from literature are not conclusive in this respect. Previous studies on second order nonlinearity in silicon nitride reported the observation of a strong SHG from PECVD silicon nitride films grown on fused silicon oxide substrate [16], where the nonlinearity was assigned to a SiN_x bulk origin. On the other hand, an interface-induced $\chi^{(2)}$ was reported in thin film Bragg reflectors fabricated in various compositions of amorphous silicon nitride [17], in high-quality amorphous silicon nitride (a-$Si_{1-x}N_x$:H) Fabry-Perot microcavities [18] and in multi-layer silicon-oxy-nitride (SiON) waveguides [19]. Furthermore, a SH signal was generated in PECVD silicon nitride ring resonators [15], where the nonlinearity was attributed to the interface between the silicon nitride and the silicon oxide. In our case, however the conversion efficiency does not seem to depend on the layer thickness of SiN_x: Sample SiN1 (500nm SiNx) and Sample SiN2 (50nm SiNx) show basically the same conversion efficiency. Thus a contribution from a silicon nitride bulk $\chi^{(2)}$ seems negligible in our case, so that the Si/SiN_x-interface remains as possible source for additional SHG enhancement.

4. Charge state and electric field at the interface

To clarify the impact of the SiN_x/Si-interface we investigated the charge state of the SiN_x and SiO_2 layers. For this purpose Capacitance-Voltage (C-V) measurements were carried out at SiN_x-layers and a SiO_2 –layer, which were deposited in the same way as the waveguide samples investigated here. **Figure 6** shows the C-V-curves for the sample coated with 57nm

of quasi-unstressed SiN_x-layer (representing the conditions at waveguide sample SiN0) and for a 482nm thick thermal oxide layer (representing the conditionas at waveguide sample SiO2). Both curves show a steep increase in capacitance when a sufficient negative potential is applied to the top aluminium contact. This corresponds to the transition from depletion towards accumulation of charges in the Si at the Si/insulator interface. However the onset of this rise is quite different for both samples. Especially for the SiN_x-coated sample a strong negative potential of around -4V is necessary to start accumulation. This is already a qualitative indication, that the SiN_x-layer carries a lot of fixed positive charges. Following the classic procedure for the evaluation of these C-V curves (see supplementary information A and [26]), the areal density of these positive fixed charges can be derived from the position of the flat bend voltage V_{fb} and was determined to $\sigma_{fix\text{-}SiN0}= 2\cdot10^{12}cm^{-2}$ and $\sigma_{fix\text{-}SiO2}= 9.9 \cdot10^{10}$ cm^{-2} for the SiN_x-layer and the SiO_2 layer, respectively. The high concentration of positive fixed charges in the SiN_x-layer is remarkable. Furthermore we conclude that the majority of these charges must be located close to the Si/SiN_x-interface since C-V-measurements for the SiN_x-layers with 500nm thickness (representing the samples SiN1 and SiN4) resulted in a similar overall areal charge density of $\sigma_{fix\text{-}SiN1}= 1.1\cdot10^{12}cm^{-2}$ although the layer was an order of magnitude thicker than the SiN0-like sample (see supplementary information B). These positive fixed charges will drive the holes in the p-type silicon away from the interface leading to a majority carrier depletion. An effective negative space charge builds up in the Si, which has the same value as the fixed charges in the SiN_x- or SiO_2 layer.

From the knowledge of the p-type doping level ($7x10^{15}$ cm^{-2}) the relationship between the surface potential ϕ_s at the interface and the areal charge density within the silicon can be derived (**Figure 7a**). For charge densities which correspond to $\sigma_{fix\text{-}SiO2}$ the silicon is in depletion, which results in a maximum electric field of E_{max}^{int}=$1.5x10^4$ V/cm at the interface. Assuming a constant negative charge density within the depletion layer of N_A=$7x10^{15}cm^{-2}$

(negatively charge acceptors), a moderate depletion width of 141nm results (Fig. 7b). The much higher positive fixed charge density of the nitride layers on the other hand leads to a considerably stronger electric field at the interface: E_{max}^{int}=3x10^5 V/cm (Fig. 7c). This causes a densely charged inversion layer at the interface with a width of about 10nm. Although the electric field drops fast in this inversion layer, a sizeable field of the order of 10^4 V/cm still penetrates up to 350nm deep into the silicon, which corresponds to the maximum width of the adjacent depletion layer.

The dc-electric field in depletion and inversion layers has an impact on the optical properties. It breaks the centrosymmetry in the silicon band structure, so that electric field induced second harmonic generation (EFISH) can emerge from there. Since the dc-electric fields in the inversion and depletion layer of the nitride covered samples are considerably higher than in the oxide coated case, a much stronger EFISH-effect is expected for the SiN_x-coated Si waveguides. Furthermore the penetration depth of the dc-electric fields into the silicon is larger for the SiN_x-coated samples, since its depletion width is more than double the depletion width for the oxide coated samples.

Note, that the EFISH-effect is a known effect in silicon and was already thoroughly investigated at MOS-capacitors [27-30] where a voltage was applied externally across the MOS-structure generating electric fields of the order of 10^5 V/cm in the silicon space charge layer. As a result, a manifold enhancement of the SH signal was observed in reflection from the dielectric/semiconductor interface of the MOS-structure.

We suggest that in our waveguides the same EFISH effect contributes to the SHG signal measured in transmission, but that the electric field is internally created by the fixed positive charges within the coatings.

The EFISH effect is actually a third order nonlinear effect, which is based on the $\chi^{(3)}$ of a material and the application of a dc-electric field. The nonlinear polarisation P^{NL} can be written as [31]:

$$P^{NL} = 3\varepsilon_0 \; \chi^{(3)} E_{dc} E^2(\omega). \qquad (5)$$

When $E(\omega)$ represents the oscillating electric field of the pump light, the resulting nonlinear polarization will have a component at 2ω - the SHG signal. To compare the possible strength of this quasi-second order nonlinearity with the classic values for $\chi^{(2)}$ of other materials, a quasi-$\chi^{(2)}$ $\left(\chi^{(2)}_{quasi}\right)$ can be defined in our case as:

$$\chi^{(2)}_{quasi} = \chi^{(3)} \; E_{dc} \qquad (6)$$

A $\chi^{(3)}$=3.82x10^{-11} m^2/V^2 for silicon at pump wavelengths around 2.2 μm can be derived from the silicon Kerr coefficient n_2=9x10^{-14} cm^2/W, which was determined by a z-scan technique [32]. From this a maximum $\chi^{(2)}_{quasi}$=11.4 pm/V is obtained for the maximum dc-electric field of 3x10^7 V/m at the SiN_x/Si interface. For the lower electric field at the SiO_2/Si-interface (6) yields $\chi^{(2)}_{quasi}$=0.6 pm/V. Although these numbers can only represent estimates (since they are based on the n_2-values which were determined for the case when all three electric field factors in (5) have the same high frequency ω), they nevertheless indicate that a quasi-$\chi^{(2)}$ with values on the order of classic second order nonlinear materials can be generated by the observed dc-electric fields.

Since the areal charge density is similar for all nitride coated samples we might conclude that all our investigated SiN_x-layers experience the same high level of the EFISH-effect. This further supports our earlier assumption that we can add the same offset in SHG-enhancement (now known as EFISH) to the conversion efficiencies of all SiN_x-covered samples in Fig. 5. With this we could show that inhomogeneous strain and interface charges are both possible sources for enhanced SHG in silicon waveguides. A further increase in inhomogeneous strain (represented by even stronger stress/strain gradients) and highly charged interfaces will be a way to increase the generated second order nonlinearity further.

When our results are compared with the relevant literature on SHG reflection measurements on MOS structures, it has to be emphasized that in our case pump light and SH-light are in the infrared with photon energies even below the indirect Si-bandgap ($\lambda_{2\omega}$ >1200nm). The observed resonant enhancement of the SHG, when the photon energy of the second harmonic radiation approaches the direct bandgap of Si [29],[30], does therefore not appear in our experiments. Furthermore effects like the shift of the flatband voltage due to the screening of the electric field by photoexcited free carriers [33] can also be neglected in our case, as the low energy IR photons of pump and second harmonic radiation can not excite electron hole pairs. On the other hand contributions to the SHG from stress-induced changes to the second order bulk quadrupole susceptibility (as suggested in [34]) can not be totally excluded, since the observed rise of the SHG efficiency with the integrated stress gradient could partly be caused by the overall rise of the stress/strain level in Si too. Further studies, which focus on a comparison of the SHG from homogeneously and inhomogeneously strained waveguide structures, are necessary to clarify this point.

5. Conclusion

In conclusion, the influences of the inhomogeneous stress and the presence of a silicon nitride layer on the second order nonlinearity in silicon waveguides could be separated. Both schemes enhance the nonlinear optical response of the waveguides. While the stressed layers create an inhomogeneous strain field within the silicon and break its centrosymmetry in this way, the enhancement due to the SiN_x alone was attributed to a high level of fixed positive charges close to the Si/SiN_x-interface, which lead to a strong electric field in the silicon near the interface and cause a pronounced EFISH contribution. It was also found, that both contributions add up constructively, which allows the combination of both methods to further enhance the effective nonlinearity of the waveguides in the future.

6. Experimental Section

Sample preparation: The Si-reference waveguide was fabricated in a classic way by first defining the strip waveguide photolithographically on the Si-device layer of the SOI-substrate and then etching the wafer in an inductively coupled reactive ion etching system (ICP-RIE "Plasmalab 100") using a SF_6/C_4H_8 gas mixture. The remaining resist was finally removed in an oxygen plasma. The oxide covered Si-waveguides were fabricated by first thermally oxidizing the SOI substrates at 1050°C for 1h in water vapour (wet oxidation) thereby growing a 500nm thick silicon dioxide layer. Afterwards the waveguides were structured as before forming the oxide covered waveguides. The SiN_x-covered samples SiN0,SiN1, SiN2 and SiN4 were fabricated by depositing the SiN_x-layers using dual frequency sputtering on the SOI. During this sputter process the stoichiometry of the deposition plasma remains constant but the radio frequency is modulated allowing the deposition of differently stressed layers. For the samples SiN1 and SiN2 the nitride layer was deposited before the waveguide etching while for the samples SiN0 and SiN4 first the waveguides were structured (similar like SiRef) and afterwards the SiN_x was deposited leading to a more conformal SiN_x-coating for SiN0 and SiN4.

The waveguides of SiN3 were first etched and afterwards covered by SiNx using a low pressure chemical vapour process (LPCVD) leading to the conformal coating of highest stress.

Measurement of Second harmonic generation (SHG):

The pump laser was coupled in and out of the waveguides using gold coated reflecting mirror objectives. The laser spot size at the entrance facet of the waveguide was about 4µm in diameter and the pump laser was polarized horizontally. By imaging first the transmitted pump beam onto an IR Vidicon Camera (sensitive in the spectral range 0.75- 2.25 um), the best waveguide coupling and the predominant excitation of the fundamental TE_{00} waveguide mode was assured. This coupling results in insertion losses on the order of ~12-15 dB.

Subsequently the signal from the waveguide was recorded by a Fourier transform infrared spectrometer (FTIR) equipped with a LN_2-cooled InSb-detector, which allowed simultaneous recording of the signal at fundamental and SH wavelengths. The linear propagation losses for the SH-wavelength were only 1-3dB/cm, since for the SH-Wavelengths >1200nm investigated by us interband absorption does not yet occur and the linear waveguide losses are governed by free carrier intraband absorption and scattering from waveguide surface roughness.

C-V-measurements: Si bulk wavers with a similar doping level (7×10^{15} cm^{-3}) as the SOI-waveguides were used and SiN_x-layers as well as a wet-thermal oxide layer were deposited/grown under the same conditions as the waveguide samples. Afterwards aluminium contact pads with different rectangular areas ranging from 350µm x350µm to 950µm x 950µm were fabricated using photolithography and a lift-off process. Subsequently the large area samples (ca. 10cm^2) were placed on a metal plate which functioned as the bottom contact, while a needle contact was applied at the Al-pads. The C-V curves were measured with an LCR-meter at several ac-frequencies. Here only the 1MHz measurements are shown.

Supporting Information
Supporting Information is available from the Wiley Online Library or from the author.

Acknowledgements

C. Schriever and J. Schilling would like to thank the Federal Ministry for Education and Research ("Bundesministerium für Bildung und Forschung") for their financial support within the Centre for Innovation Competence SiLi-nano (project number 03Z2HN12) and Prof. Ulrich Hilleringmann for providing most of the SiN_x-depositions. F. Bianco, M. Cazzanelli, M. Ghulinyan and L. Pavesi would like to thank the Provincia Autonoma di Trento and Fondazione Cariplo for their financial support in the framework of the FUPAT- NAOMI

project and by the grant number 2009-2730, respectively. Author 1 and Author 2 contributed equally to this work.

Received: ((will be filled in by the editorial staff))
Revised: ((will be filled in by the editorial staff))
Published online: ((will be filled in by the editorial staff))

[1] C. K. J. Leuthold and W. Freude, Nature Photon. **4**, 535 (2010).

[2] C. Koos, L. Jacome, C. Poulton, J. Leuthold, and W. Freude, Opt. Express **15**, 5976 (2007).

[3] C. Koos, P. Vorreau, T. Vallaitis, P. Dumon, W. Bogaerts, R. Baets, B. Esembeson, I. Biaggio, T. Michinobu, F. Diederich, W. Freude, and J. Leuthold, Nat. Photonics **3**, 216 (2009).

[4] C. Schriever, C. Bohley, and J. Schilling, Photonics and Nanostructures - Fundamentals and Applications **10**, 312 (2012).

[5] S. Mitchell, M. Mehendale, D. Villeneuve, and R. Boukherroub, Surface Science **488**, 367 (2001).

[6] J. E. Mejia, B. S. Mendoza, M. Palummo, G. Onida, R. Del Sole, S. Bergfeld, and W. Daum, Phys. Rev. B**66**, 195329 (2002).

[7] J. E. Sipe, D. J. Moss, and H. M. van Driel, Phys. Rev.B **35**, 1129 (1987).

[8] N. Bloembergen, Appl. Phys. B **68**, 289 (1999).

[9] J. Y. Huang, Jpn. J. Appl. Phys. **33**, 3878 (1994).

[10]S. V. Govorkov, V. I. Emel'yanov, N. I. Koroteev, G. I. Petrov, I. L. Shumay, and V. V. Yakovlev, JOSA B **6**, 1117 (1989).

[11]C. Schriever, C. Bohley, and R. B. Wehrspohn, Opt.Lett. **35**, 273 (2010).

[12] M. Cazzanelli, F. Bianco, E. Borga, G. Pucker, M. Ghulinyan, E. Degoli, E. Luppi, V. V´eniard, S. Ossicini, D. Modotto, S. Wabnitz, R. Pierobon, and L. Pavesi, Nat. Mater. **11**, 148 (2011).

[13] R. S. Jacobsen, K. N. Andersen, P. I. Borel, J. Fage-Pedersen, L. H. Frandsen, O. Hansen, M. Kristensen, A. V. Lavrinenko, G. Moulin, H. Ou, C. Peucheret, B. Zsigri, and A. Bjarklev, Nature **441**, 199 (2006).

[14] B. Chmielak, M. Waldow, C. Matheisen, C. Ripperda, J. Bolten, T. Wahlbrink, M. Nagel, F. Merget, and H. Kurz, Opt. Express **19**, 17212 (2011).

[15] J. S. Levy, M. A. Foster, A. L. Gaeta, and M. Lipson, Opt. Express **19**, 11415 (2011).

[16] T. Ning, H. Pietarinen, O. Hyvarinen, J. Simonen, G. Genty, and M. Kauranen, Appl. Phys. Lett. **100**, 161902 (2012).

[17]S. Lettieri, S. D. Finizio, P. Maddalena, V. Ballarini, and F. Giorgis, Appl. Phys. Lett. **81**, 4706 (2002).

[18] E. Descrovi, C. Ricciardi, F. Giorgis, G. L´erondel, S. Blaize, C. X. Pang, R. Bachelot, P. Royer, S. Lettieri, F. Gesuele, P. Maddalena, and M. Liscidini, Opt. Express **15**, 4159 (2007).

[19] D. F. Logan, A. B. A. Dow, D. Stepanov, P. Abolghasem, N. P. Kherani, and A. S. Helmy, Appl. Phys. Lett. **102**, 061106 (2013).

[20] L. Vanzetti, M. Barozzi, D. Giubertoni, C. Kompocholis, A. Bagolini, and P. Bellutti, Surf. Interface Anal. **38**, 723 (2006).

[20] I. D. Wolf, H. E. Maes, and S. K. Jones, Journal of Applied Physics **79**, 7148 (1996).

[21] S. Narayanan, S. R. Kalidindi, and L. S. Schadler, Journal of Applied Physics **82**, 2595 (1997).

[22] F. Bianco, K. Fedus, F. Enrichi, R. Pierobon, M. Cazzanelli, M. Ghulinyan, G. Pucker, and L. Pavesi, Semicond. Sci. Technol. **27**, 085009 (2012).

[23] J. de Boor, N. Geyer, J. V. Wittemann, U. G¨osele, and V. Schmidt, Nanotechnology **21**, 095302 (2010).

[24] B. E. Warren, *X-ray Diffraction* (Courier Dover Publications, 1969).

[25] U. Pietsch, V. Hol´y, and T. Baumbach, *High-Resolution X-Ray Scattering - From Thin Films to Lateral Nanostructures* (Spinger-Verlag, 2004).

[28] O. A. Aktsipetrov, A. A. Fedyanin, A. V. Melnikov, E. D. Mishina, A. N. Rubtsov, M. H. Anderson, P. T. Wilson, M. ter Beek, X. F. Hu, J. I. Dadap, and M. C. Downer, Phys. Rev. B **60**, 8924 (1999).

[27] O. A. Aktsipetrov, A. A. Fedyanin, E. D. Mishina, A. N. Rubtsov, C. W. van Hasselt, M. A. C. Devillers, and T. Rasing, Phys. Rev. B **54**, 1825 (1996).

[26] S.M.Sze, Kwok K Ng, *Physics of Semiconductor devices*, 3rd Ed.Wiley, Hoboken, NJ, USA **2007**

[32] A. D. Bristow, N. Rotenberg, and H. M. van Driel, Applied Physics Letters **90**, 191104 (2007);

[31] R.W.Boyd, *Nonlinear Optics,* 3rd Ed., Elsevier, Academic Press, London, UK **2008**.

[33] J. I. Dadap, P. T. Wilson, M. H. Anderson, M. C. Downer, and M. Ter Beek, Opt. Lett.**22**, 901–3 (1997).

[29] P. Godefroy, W. de Jong, C. W. van Hasselt, M. a. C. Devillers, and T. Rasing, Appl. Phys. Lett. **68**, 1981 (1996).

[30] J. Dadap, X. Hu, M. Anderson, M. Downer, J. Lowell, and O. Aktsipetrov, Phys. Rev. B. Condens. Matter **53**, R7607–R7609 (1996).

[34] O. a. Aktsipetrov, V. O. Bessonov, T. V. Dolgova, and a. I. Maidykovskii, JETP Lett. **90**, 718–722 (2010).

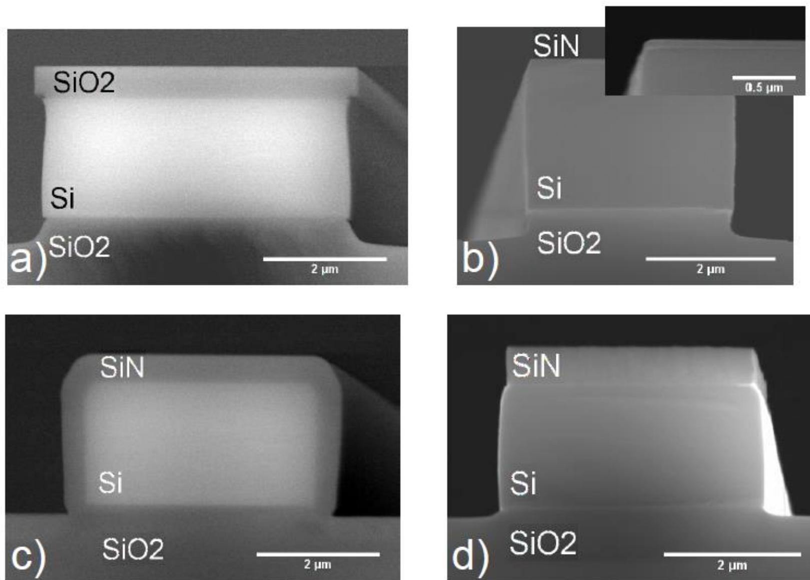

Figure 1. Scanning Electron Microscopy (SEM) images of the investigated waveguide facets. a) covered with 500 nm SiO_2 (named SiO2), b) covered with 50 nm SiN_x layer (named SiN2), c) completely coated with 500 nm SiN_x (named SiN4) and d) covered with 500 nm SiN_x (named SiN1)

Table 1. Parameters of the samples investigated here. The reported stress values were obtained by wafer bow measurement on complete wafers coated under identical conditions as the respective samples. Negative stress values describe compressively stressed layer resulting in tensile stress in the silicon and vice versa.

Sample Layer	SiRef	SiO2 top	SiN0 compl.	SiN1 top	SiN2 top	SiN3 top	SiN4 compl.
Thickn. [nm]	-	500	50	500	50	150	500
Layer stress [MPa]	-	-300	-7	+226	-880	+1200	+226
Integrated stress gradient Σ		3197	383	1535	1559	4504	821

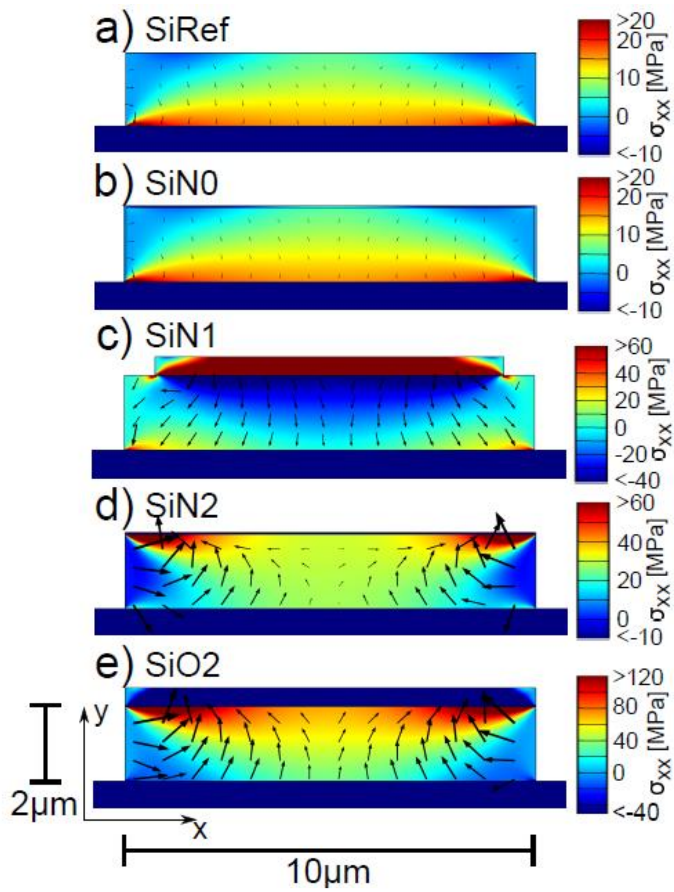

Figure 2. Simulated distribution of the stress component σ_{xx} along the cross section of 10 µm wide waveguides for sample a) *SiRef*, b) *SiN0*, c) *SiN1*, d) *SiN2* and e) *SiO2*, as well as the resulting stress gradient (arrows)

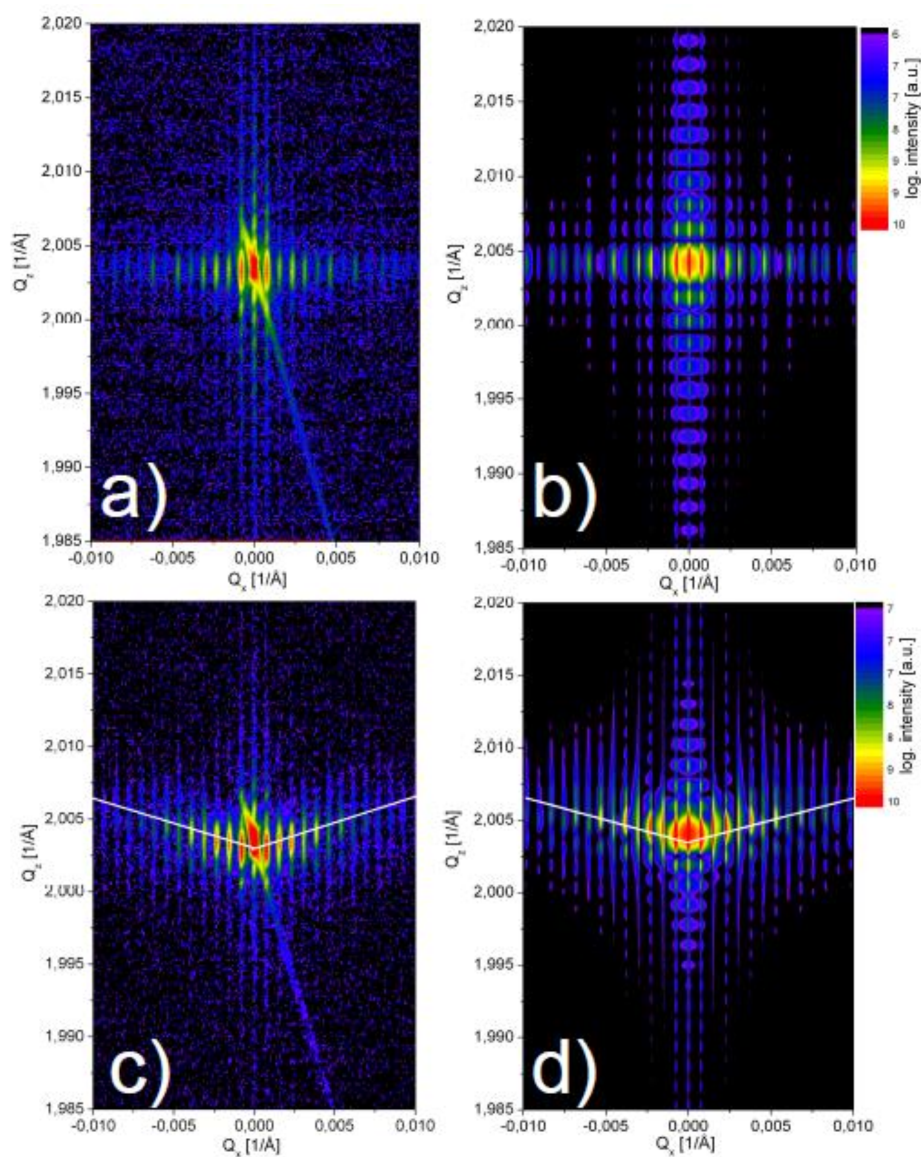

Figure 3. Comparison between experimentally (left) and numerically (right) determined reciprocal space maps (RSM) of the Si (111) reflex. In case of a stressing layer the diffracted intensity shifts to higher Q_z values (white line). The additional feature in a) and c) represents the analyzer streak related to the x-ray setup. The strong agreement of the RSM confirms the accuracy of the FEM model used for the calculations.

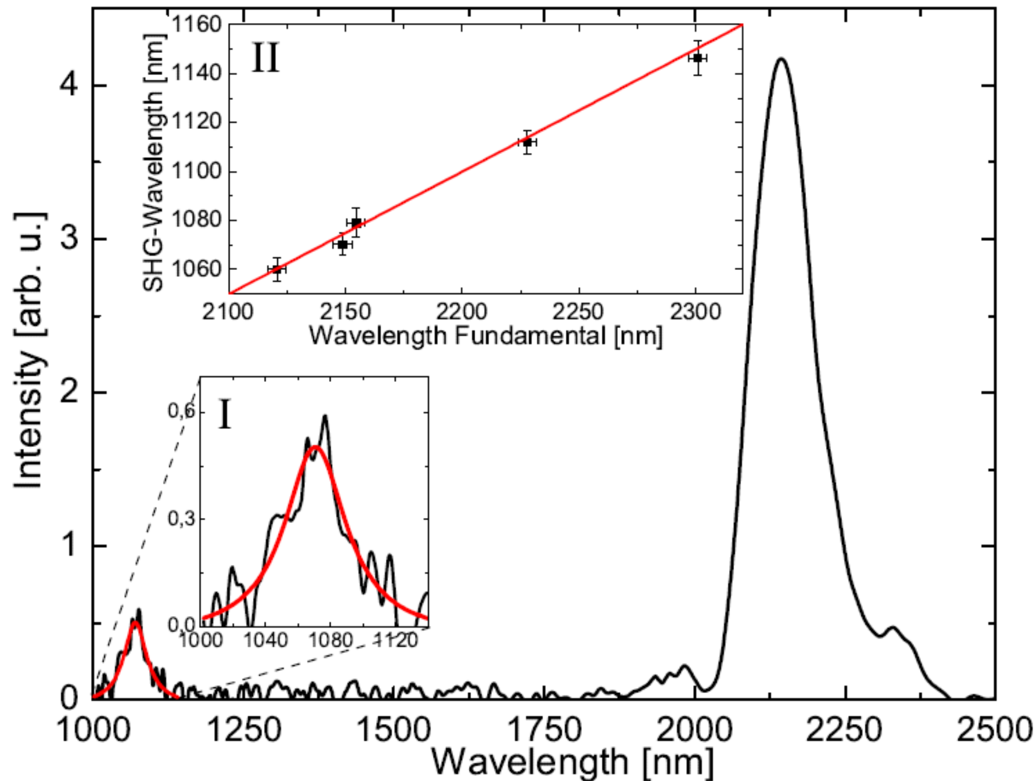

Figure 4. SHG measurements of a 10µm wide waveguide of sample SiO2 showing peaks at the fundamental λ_{ω} = 2.14 μm) and SH wavelengths $\lambda_{2\omega}$ = 1.07 μm). The coupled average power of the fundamental beam was about 0.15µW. Inset I shows the zoom of the SH peak, where the red line is the fitted Gaussian curve. Inset II shows the wavelength tunability of the SH signal. The red line is the expected relationship between $\lambda_{2\omega}$ and λ_{ω}

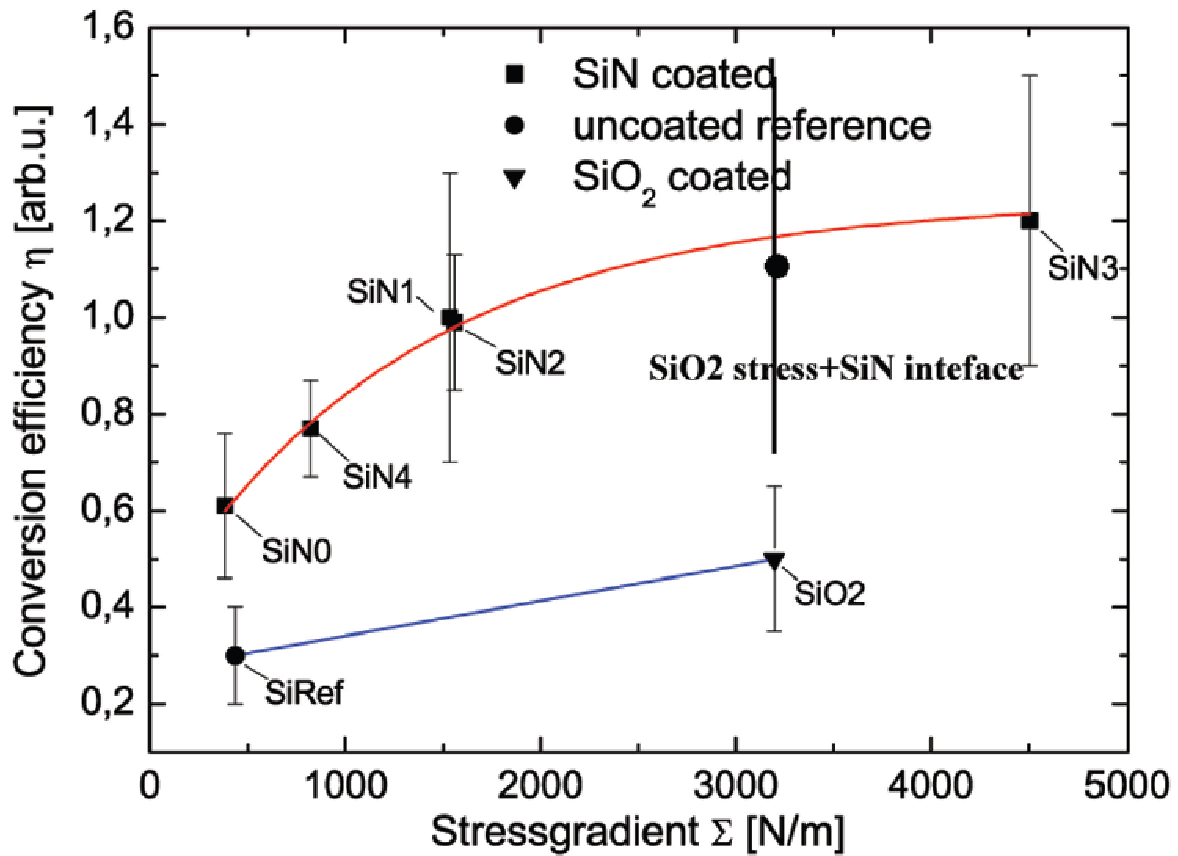

Figure 5. Dependence of the experimentally determined nonlinear conversion efficiency η on the total stress gradient Σ for 10μm wide waveguides under different stressing conditions. The lines are guides to the eye.

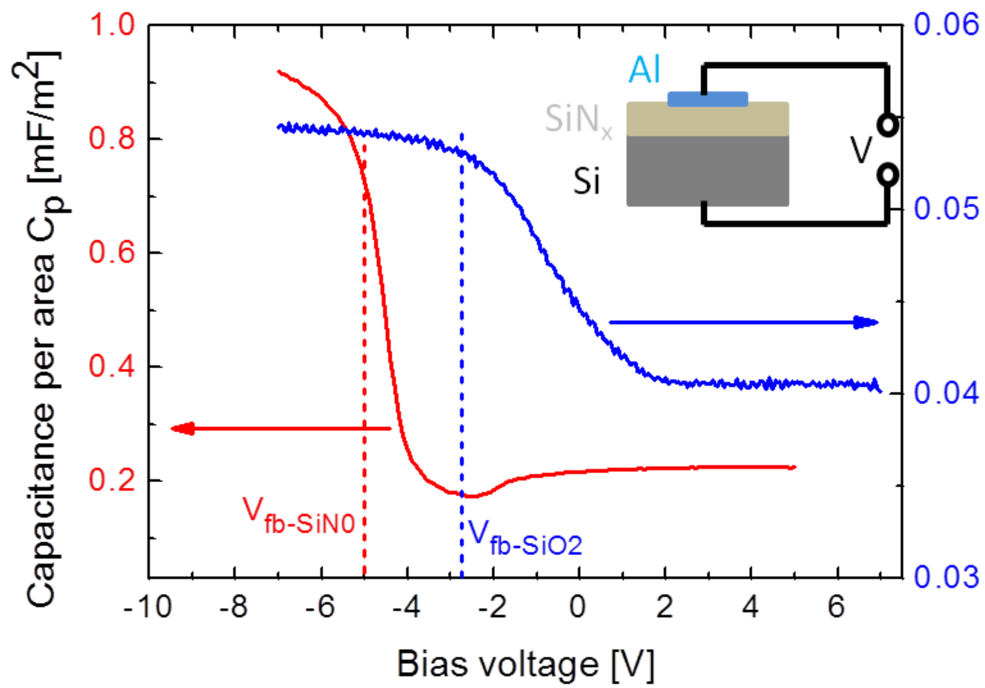

Figure 6. C-V measurement for SiN_x- and SiO_2 layers on a 2.5 Ohm*cm p-type Si waver. Red (left scale): 57nm thick quasi-unstressed (-7MPa) SiNx-layer, Blue (right): 482nm thermal SiO_2. Inset: Measurement geometry with Al-top contact on SiN_x or SiO_2-layer on Si waver.

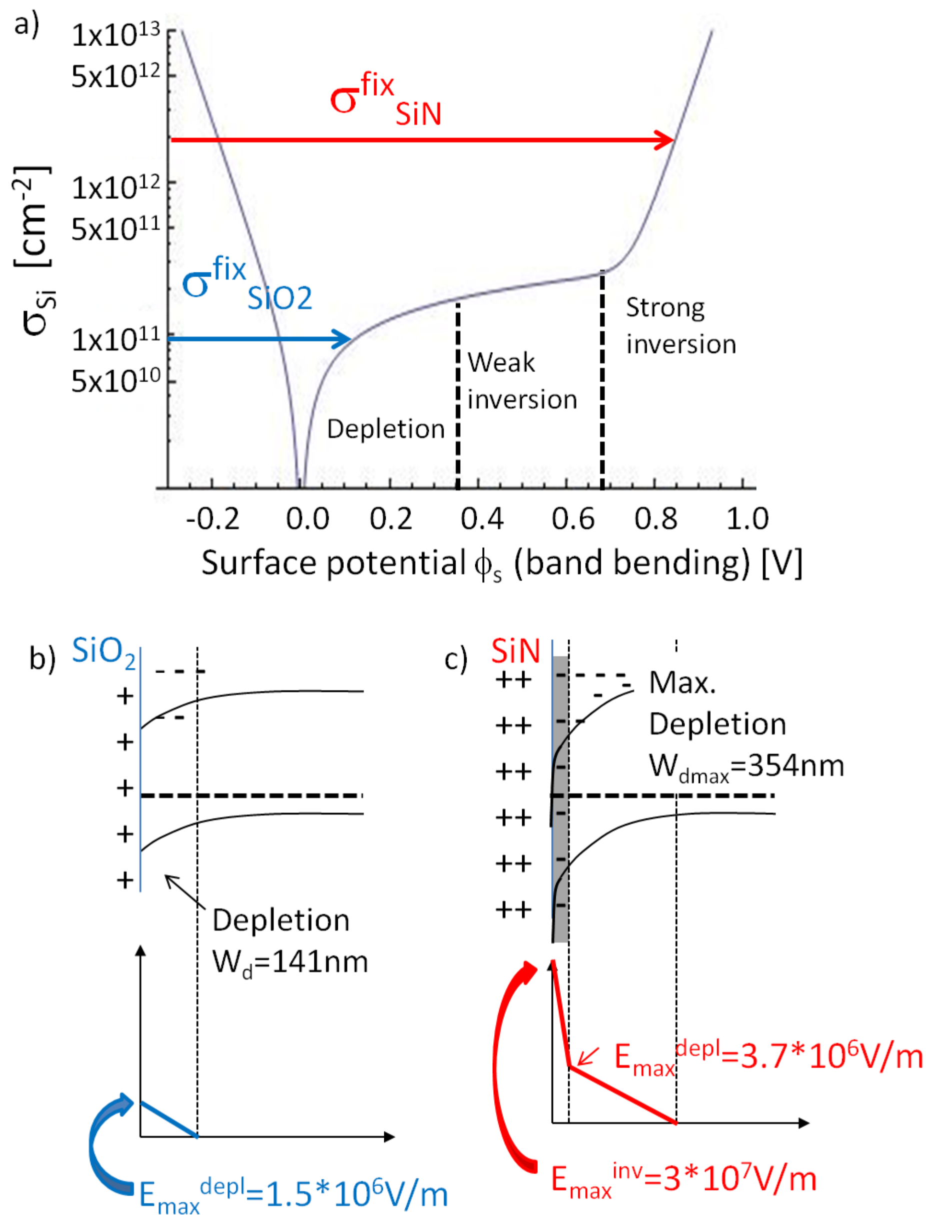

Figure7. Charge conditions at the Si/insulator interface a) Charge on the Si-side of the interface depending on the surface potential. The lower level fixed positive charges in the oxide causes only a depletion layer in the Si, while the higher charge density in the nitride drives the Si in inversion b) Band bending near the SiO_2/Si-interface for depletion. The "+" indicate the positive fixed charges in the oxide, while the "-" are the resulting negative counter charges in the depletion layer in the Si. c) Band bending near the SiN_x/Si-interface for inversion. After a densely charged inversion layer (grey shaded area) a depletion layer of maximum width 350nm follows.

((Supporting Information can be included here using this template))

Copyright WILEY-VCH Verlag GmbH & Co. KGaA, 69469 Weinheim, Germany, 2013.

Supporting Information

A) Derivation of fixed charge densities from C-V curves

Clemens Schriever, Federica Bianco, Massimo Cazzanelli, Mher Ghulinyan, Christian Eisenschmidt, Georg Schmidt, Johannes de Boor, Alexander Schmid, Johannes Heitmann, Lorenzo Pavesi, Jörg Schilling**

In the following a short description is given, how the fixed positive charge density can be obtained from the C-V-curves. For more details see [26]

To obtain the fixed charge density first the flatband voltage of the Metal-insulator-semiconductor (MIS)-structure has to be determined. First the capacitance at the flat band condition has to be found. It is defined as

$$C_{FB} = \frac{\varepsilon_0 \varepsilon_{Si} \varepsilon_{SiN}}{\varepsilon_{Si} d + \varepsilon_{SiN} L_D} \quad (1‘)$$

where L_D describes the Debyelänge $L_D = \sqrt{\frac{kT\varepsilon_0\varepsilon_{Si}}{q^2 N_A}}$, N_A ist he doping level, q the elementary charge, T the temperature and $\varepsilon_{Si}, \varepsilon_{SiN}$ the dielectric constants of silicon and SiNx respectivelyit. d- is the layer thickness of the insulating layer. The dielectric constant of the insulating layer can be derived from the capacitance in accumulation (at strongly negative biases), known metal-contact area and the layer thickness.

When CFB is calculated, the flatband voltage is derived from the C-V-curve. Using

$$V_{FB} = \phi_{ms} - \frac{Q_f}{C_i} \quad (3‘)$$

where ϕ_{ms} describes the difference in work functions between the metal contact and the semiconductor , finally the fixed charges

$$Q_f = C_i(\phi_{ms} - V_{FB}) \quad (4')$$

Since C_i is mainly taken as a capacitance/area, Q_f corresponds actually to the σ_{fix} appearing in the paper.

For a semiconductor in depletion the width of the depletion (space charge) layer is calculated as follows:

$$W_d = \sqrt{\frac{2\varepsilon_0 \varepsilon_{si} \phi_S}{qN_A}} \quad (5')$$

where ϕ_S is the surface potential at the interface insulator/Si. If however an inversion layer starts to build up, the width of the space charge layer becomes a maximum at

$$W_{d-\max} = \sqrt{\frac{4\varepsilon_0 \varepsilon_{si} kT \ln(N_A/n_i)}{q^2 N_A}} \quad (6')$$

where n_i is the intrinsic carrier concentration of the semiconductor.

B) C-V measurement for SiNx-covered Si under mechanical stress

To also check the charge state at the stressed SiNx/Si interface, C-V measurements were carried out for stressed SiNx/Si interfaces, which were created by the same SiNx-depositions like the waveguide samples. Fig. S1 shows the C-V curve for the SiNx/Si interface with a nominal 500nm thick SiNx layer (exact thickness 493nm) exhibiting a tensile stress of σ=+226MPa. This situation corresponds to the waveguide samples SiN1 and SiN4. Although the noise level is more pronounced due to the smaller capacitance values (which are a result of the relatively thick dielectric SiNx-layer), the flatband voltage can be determined to V_{fb}=-17V. Following the analysis described in section A) a fixed charge level of $\sigma_{fix-SiN1}$= $1.1\cdot10^{12}$cm^{-2} is derived. This demonstrates that the fixed charge state of the quasi-unstressed and stressed SiNx-layers is similar. Since the charge level of thick and thin SiNx-layers is

similar we can conclude that the majority of fixed charges are situated (within the SiNx) close to the SiNx/Si interface as it was already pointed out in the article.

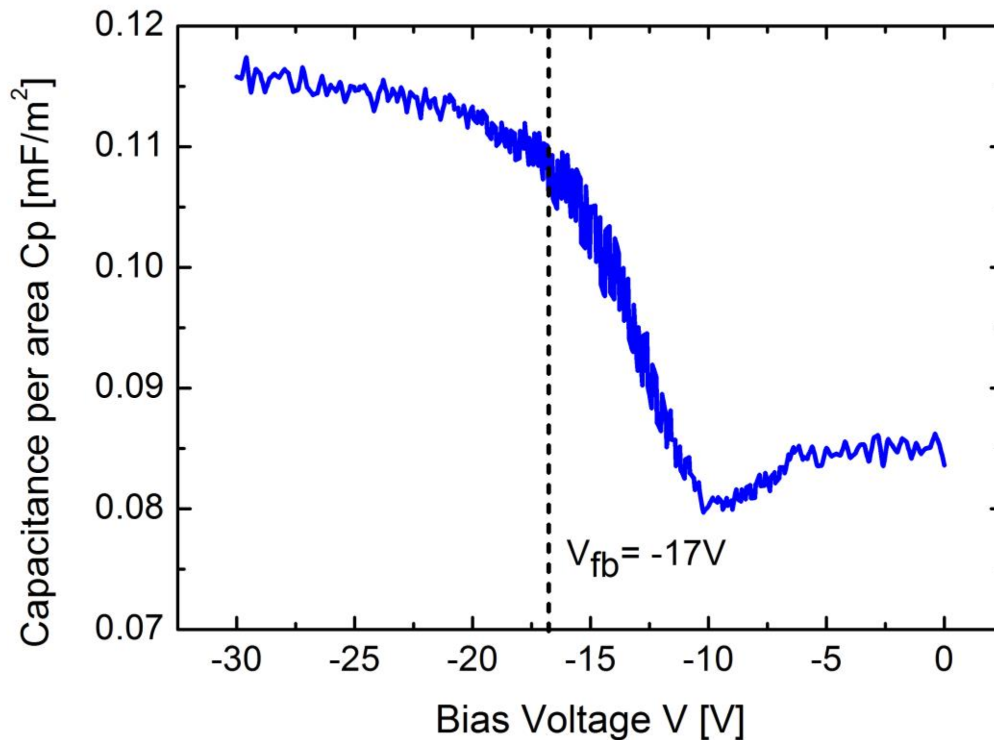

Fig. S1: C-V- measurement for a stressed SiNx/Si interface with a SiNx-layer stress of σ_{SiNx}=+226MPa corresponding to the situation of the waveguide samples SiN1 and SiN4. Due to the relatively large thickness of nominal 500nm of the SiNx-layer (exact thickness 493nm), the capacitance values are small and the flatband voltage is considerably shifted to negative values. However the analysis according to section A) reveals a charge level similar to the quasi-unstressed SiNx- layer shown in Fig. 6.